Open access • Journal Article • DOI:10.1088/1361-6439/AB4527

Design and fabrication strategy for an efficient lead zirconate titanate based piezoelectric micromachined ultrasound transducer — Source link

Sina Sadeghpour, Michael Kraft, Robert Puers

Institutions: Katholieke Universiteit Leuven

Published on: 04 Oct 2019 - Journal of Micromechanics and Microengineering (IOP Publishing)

Topics: Lead zirconate titanate, Transducer and Piezoelectricity

PAPER

Design and fabrication strategy for an efficient lead zirconate titanate based piezoelectric micromachined ultrasound transducer

IOP Publishing Journal of Micromechanics and Microengineering
J. Micromech. Microeng. **29** (2019) 125002 (14pp) https://doi.org/10.1088/1361-6439/ab4527

Design and fabrication strategy for an efficient lead zirconate titanate based piezoelectric micromachined ultrasound transducer

S Sadeghpour, M Kraft and R Puers

Department of Electrical Engineering (ESAT-MICAS), KU Leuven, Leuven 3001, Belgium

E-mail: sina.sadeghpour@esat.kuleuven.be

Received 4 July 2019, revised 23 August 2019
Accepted for publication 17 September 2019
Published 4 October 2019

Abstract

This paper presents the design and fabrication strategy of a lead zirconate titanate (PZT)-based piezoelectric micromachined ultrasound transducers (pMUT) with the objective of maximizing its performance. Choosing the most suitable thickness of the PZT layer, the radius of the top electrode, and the effect of the residual stress on the resonance frequency of a pMUT are investigated by finite element method (FEM) simulation and analytical equations. Three different architectures of pMUTs are presented: (i) a pMUT with a top center electrode, (ii) a pMUT with a top center and ring electrode, (iii) a pMUT with a patterned PZT layer. All three pMUT architectures were fabricated and their displacement response, resonance frequency, and Q-factor are compared. The fabricated pMUT in all three architectures has a radius of 205 μm, a Si membrane thickness of 6 μm, and a PZT thickness of 1 μm. The experimental results were compared to FEM simulation. The proposed architectures have a displacement response of 6.6 μm V^{-1}, 7.5 μm V^{-1}, and 8.6 μm V^{-1}, respectively, for their optimum design parameters.

Keywords: piezoelectric micromachined ultrasound transducer (pMUT), lead zirconate titanate (PZT), residual stress, sensor networks

(Some figures may appear in colour only in the online journal)

1. Introduction

During the last decade, the interest in ultrasound transducers has rapidly increased. Ultrasound transducers are used in many different applications, such as medical imaging [1], collision avoidance, underwater communication [2], and nondestructive testing in underwater sensor networks. Piezoelectric micromachined ultrasound transducers (pMUTs), due to their small size, low power consumption [3], and high element density [4] have become a promising technology as an alternative to conventional ultrasound transducers, which are mostly based on thick-film piezoelectric layers. Unlike conventional ultrasound transducers, in which the resonance frequency depends on the thickness of the piezoelectric film [5], the resonance frequency of a pMUT is dependent on its membrane thickness and also the lateral dimension. Therefore, pMUTs can be fabricated in miniaturized dimensions. For instance, for a constant frequency we can reduce the thickness and the lateral dimension of the pMUT together by lithographic resolution. This led to a growing portfolio of new applications, such as finger print sensors [6], range finding for automotive and internet of things (IoTs) [7], intravascular imaging [8, 9], high resolution 3D medical imaging [10], and low power communication for small underwater sensor nodes [11].

However, the design of an efficient pMUT is not trivial. Depending on the application, there are many parameters in the design and fabrication of a pMUT which should be optimized, such as the geometrical parameters, the thickness and diameter of the membrane of a pMUT, and the deposition parameters of the piezoelectric thin-film. There are several publications in which a specific pMUT with certain parameters

was introduced, but it was not described why and how these parameters were chosen [12, 13].

Furthermore, there are few examples of a detailed analysis of the design and fabrication of pMUTs in the literature. Akasheh *et al* presented a study based on finite element method (FEM) simulation on optimizing the geometrical parameters to maximize the coupling coefficient of a rectangular pMUT based on a thick piezoelectric film [14]. Moreover, Wang *et al* introduced a method to enhance the displacement of the membrane by etching holes on the circumferential area of the membrane, which reduces its stiffness [15]. However, the presence of these holes on the pMUT is not practical for many applications. Accordingly, Wang *et al* applied a geometrical modification on the membrane to reduce the stiffness and to increase the displacement [16]. In a more recent work, Thao *et al* and similarly Lu *et al* briefly explained what the optimum dimension of the top electrode for a circular pMUT should be [17, 18]. In addition, there are several analytical studies on the optimum dimension of the top electrode of a circular piezoelectric resonator. For instance, Sammoura *et al* found the optimum dimension of the top electrode of a circular bimorph pMUT analytically [19]. Likewise, Mo *et al* acquired the optimum top electrode dimension of a unimorph resonator for energy harvesting applications [20].

However, it has been found that there is a serious lack of a detailed and comprehensive study on a generalized method to design and fabricate pMUTs, which can be used regardless of the application. Despite the importance of several practical parameters, such as residual stress and the loading effect of the medium, they are not considered in most of the aforementioned analytical studies.

In this paper, we investigate the design and fabrication strategy of a lead zirconate titanate (PZT) based pMUT to be used in underwater and in-air applications. The displacement response of the proposed pMUT were maximized by optimizing the PZT deposition, geometrical parameters, and the fabrication procedure. PZT is used, because it has one of the highest piezoelectric coefficient among all piezoelectric materials [21]. As shown in figure 1, three different design architectures of a pMUT are introduced to improve the performance of the pMUT. Architecture (a) is the basic structure of a pMUT and is commonly used in various applications [21].

Architecture (b), in which a ring electrode is added on the circumferential area of the pMUT membrane, was used few times in the literature [22, 23]. The use of the ring electrode was motivated by the fact that actuating it by a 180° phase shifted signal produces a larger bending moment, which results in a larger displacement. Although, this is not always correct and this paper tries to investigate it in detail and compare its performance to the architecture (a).

Architecture (c), in which the PZT layer is patterned on top of the membrane, is an improved version of the one that was used by Thao *et al* [24]. Unlike the work of Thao *et al*, we could successfully pattern the PZT without any crack or delamination of the PZT layer. The introduced architecture (c) in this paper is the most efficient design, in means of performance, up to now, which can be used for underwater applications. The dynamic behavior of the pMUT with architecture (c) is discussed in detail.

All three architectures are discussed in individual sections. The pMUT design and the fabrication process are explained only once and in the section of the architecture (a), since they are common for the other two architectures.

2. Architecture (a): basic architecture of a pMUT

Figure 1(a) shows the basic architecture of a pMUT that is used in most of the reported pMUTs [21]. It consists of a membrane and a piezoelectric layer which is sandwiched by a bottom and top electrode. The top electrode has a circular shape and a radius smaller than the pMUT radius. The design and choice of the optimal radius of the top electrode, values of the thickness and radius of the pMUT membrane, and the thickness of the piezoelectric layer are discussed in this section. In section 2.1 a general approach in the design of a pMUT is followed, while a specific pMUT with a center frequency of approximately 500 kHz was fabricated and characterized. The fabricated pMUT is intended to be used for underwater and/or in-air sensor network applications, in which a communication distance range of at least 1–2 m is required. At the end the results of the fabricated pMUT are compared with the discussed design strategy.

2.1. PMUT design

In this section, the concepts behind the design and the choice of the main parameters of a general purpose pMUT are discussed. The displacement response of the pMUT membrane (Δx), which can be related to its velocity by $v = 2\pi f \Delta x$, as the figure of merit (FOM), was aimed to be maximized by optimizing the design parameters. The design procedure adopted in this work is mostly based on FEM simulations using COMSOL Multiphysics 5.4 (COMSOL Ltd., Stockholm, Sweden). Table 1 shows the material parameters that were used in the FEM simulations.

2.1.1. Defining the resonance frequency. The resonance frequency is the first criterion that should be taken into account in the design of a pMUT. Depending on the application, most of the times there is some flexibility in choosing the resonance frequency. This may help to compromise other parameters in the design procedure. The resonance frequency of a clamped single layer membrane with no residual stress can be calculated by equation (1) [25],

$$f_r = \frac{1}{2\pi}\frac{\beta^2}{a^2}\sqrt{\frac{D}{\rho'}} = \frac{1}{2\pi}\frac{\beta^2 t}{a^2}\sqrt{\frac{E}{\rho(1-\nu^2)}} \qquad (1)$$

where a is the radius of the pMUT membrane, D the flexural rigidity of the plate, ρ the volume density of the membrane material, t the thickness of the membrane, ρ' the density per unit area and is equal to ρt, E Youngs modulus, and ν the Poissons ratio. D can be obtained by equation (2) [26], where z_0 is the position of the neutral axis and can be found by

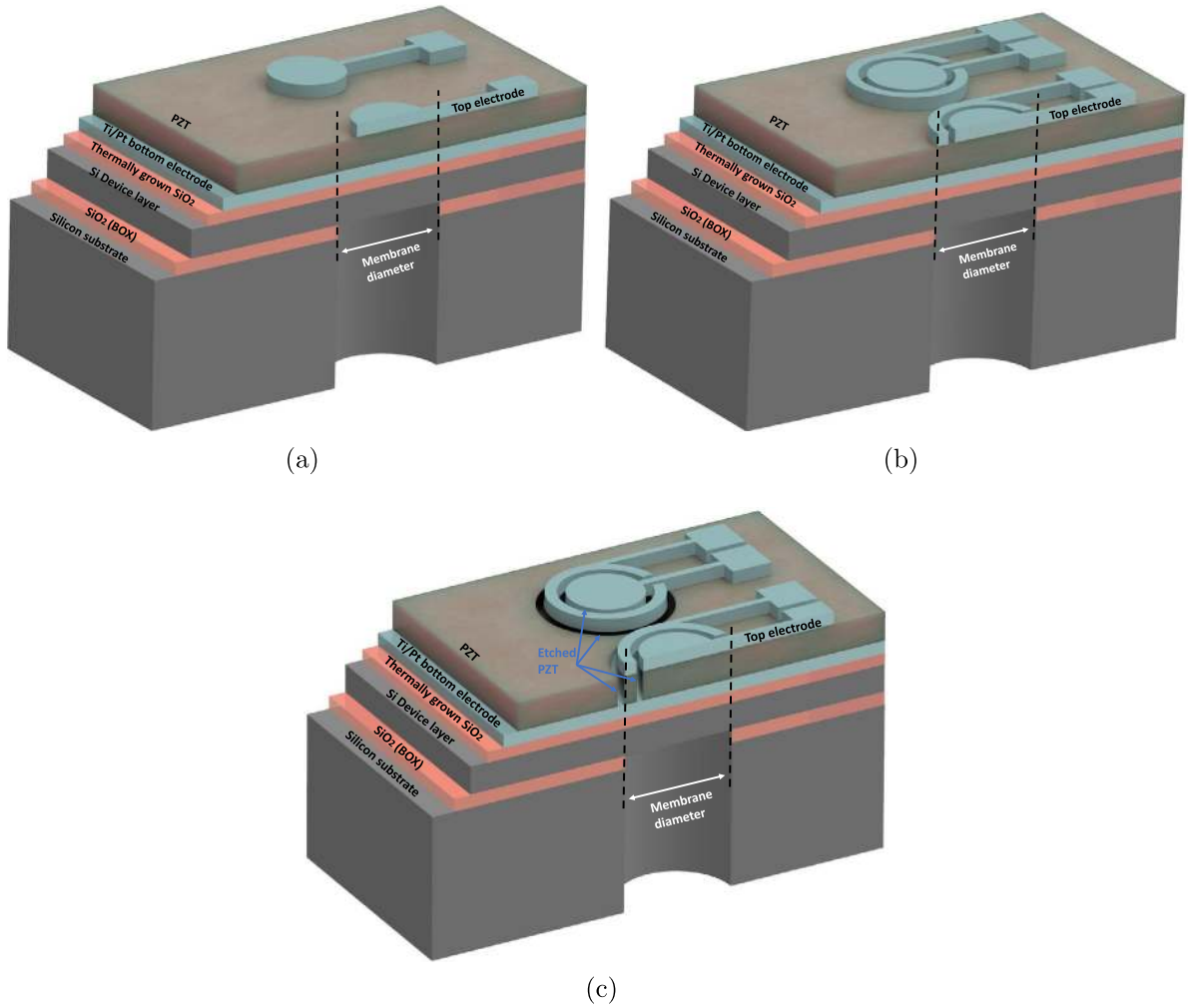

Figure 1. Illustration of the three pMUT architectures that are investigated in this paper. (a) PMUT with a center electrode (basic architecture of a pMUT). (b) PMUT with a center and ring electrode. (c) PMUT with a patterned PZT layer.

Table 1. Material parameters that were used in the FEM simulations.

Material	Density	Young's modulus	Poisson's ratio
Silicon	2300 (kg m^{-3})	170 (GPa)	0.28
PZT	7500 (kg m^{-3})	76 (GPa)	0.3

equation (3). In equations (2) and (3), the integration is over the thickness of the pMUT membrane.

$$D = \int_h \frac{E_z(z - z_0)}{1 - \nu_z^2} dz \tag{2}$$

$$z_0 = \int_h E_z(z - z_0) dz = 0. \tag{3}$$

The resonance frequency has a directly proportional relationship with the membrane thickness and an indirectly proportional relationship with the square of the membrane radius.

In a practical pMUT, however, the membrane consists of several layers, such as the piezoelectric layer and electrodes. In this case, the property of these extra layers should also be taken into account in the calculation of the resonance frequency. The resonance frequency of a multi-layer membrane is defined by equation (4), where i designates the number of each layer. In the calculation of the resonance frequency of a multi-layer membrane, E_z and ν_z in equations (2) and (3) are a function of the membrane thickness.

$$f_{r,m} = \frac{1}{2\pi} \frac{\beta^2}{a^2} \sqrt{\frac{D}{\Sigma_i \rho_i t_i}}. \tag{4}$$

If a pMUT is working in an environment other than vacuum, the mass of the medium can load the surface of the pMUT and alter the resonance frequency. It was shown that the reactive output acoustic power of a pMUT is consumed to bring the extra mass on its surface into vibration [27]. The reactive power is dominant when the radial diameter of the pMUT membrane is much smaller than the ultrasound wavelength in the medium. In other words, if $ka \ll 1$, where $k = 2\pi/\lambda$ is the wavenumber, λ is the wavelength, and a is the radius of the pMUT, most of the output acoustic power is reactive. For instance, in the majority of pMUT designs at low frequency underwater applications, the dimension of the membrane is much smaller than the wavelength [28, 29]. For the case of $ka \ll 1$, the extra loaded mass on the surface of the pMUT can be modeled as a cylinder on top of the pMUT,

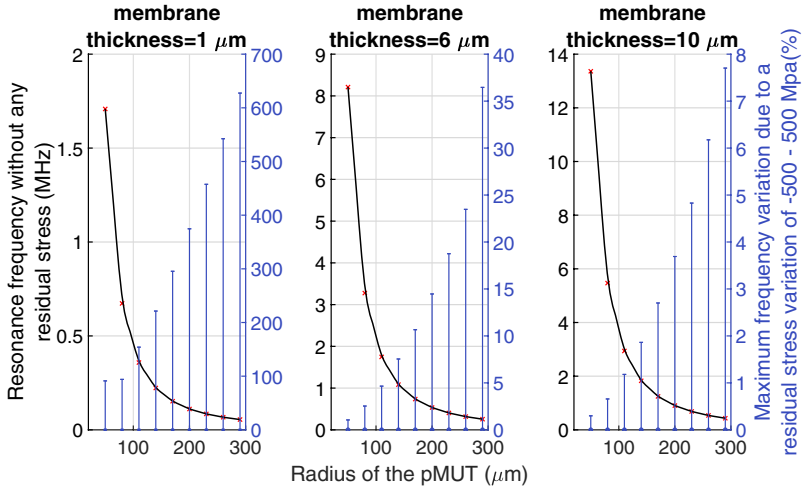

(a)

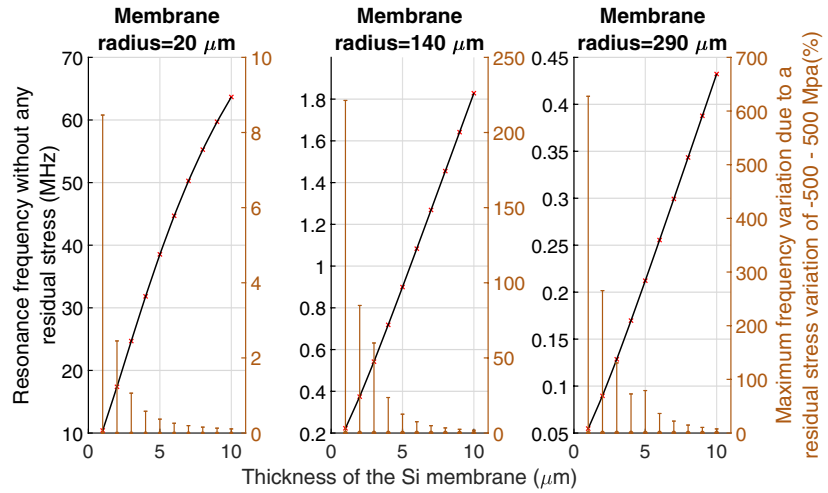

(b)

Figure 2. FEM simulation of the resonance frequency of a pMUT with 1 μm PZT as a function of (a) the radius and (b) the thickness of the Si membrane. The maximum resonance frequency variation due the residual stress variation of the PZT layer from −500 MPa to 500 MPa is shown by vertical bars on the right y-axis in percentage.

with a cross-sectional area S, (equal to the area of the pMUT membrane), and a height of $8a/3\pi$, where a is the radius of the pMUT [27]. Consequently, the extra mass of the medium on the pMUT can be calculated by equation (5), where ρ_m is the density of the medium. Accordingly, equation (4) can be redefined, as equation (6), by adding the extra mass of the medium to the mass of the pMUT membrane in order to take into account the loading effect of the working medium for $ka \ll 1$.

$$m = \rho_m S \frac{8a}{3\pi} \tag{5}$$

$$f_r = \frac{1}{2\pi}\frac{\beta^2}{a^2}\sqrt{\frac{D}{\rho'}}\left(1+\zeta\frac{\rho_m a}{\rho t}\right)^{-1/2}. \tag{6}$$

In equation (6), ζ is a correction coefficient, which is equal to 0.84. Although, depending on ka and the boundary conditions the value of ζ may differ [25, 30]. It should be noted that equation (4) is only valid for the (0,0) vibration mode. In the design of a pMUT, the diameter of the membrane should be set as close as possible to half of the wavelength (conceivably bigger) to maximize the output acoustic power and avoid the effect of the extra mass of the medium on the resonance.

The other factor which can vary the resonance frequency is the residual stress of the deposited layers. Figures 2(a) and (b) show FEM simulations of the resonance frequency of a Si membrane with 1 μm deposited PZT with respect to the radius and thickness of the Si, respectively. In these figures the vertical bars show the maximum frequency variation of the pMUT, while the residual stress of the PZT layer was changed from −500 MPa to 500 MPa. For the sake of simplicity, in the simulation, the residual stress was modeled by thermal stress. From figure 2, it can be concluded that the resonance frequency is less dependent on the residual stress of the deposited layers in case of thicker and smaller membranes. This means that the frequency variation due to the residual stress is more pronounced at lower frequencies. For instance, for a resonance frequency of lower than 100 kHz, a frequency variation of more than 600% may exist. As a general statement,

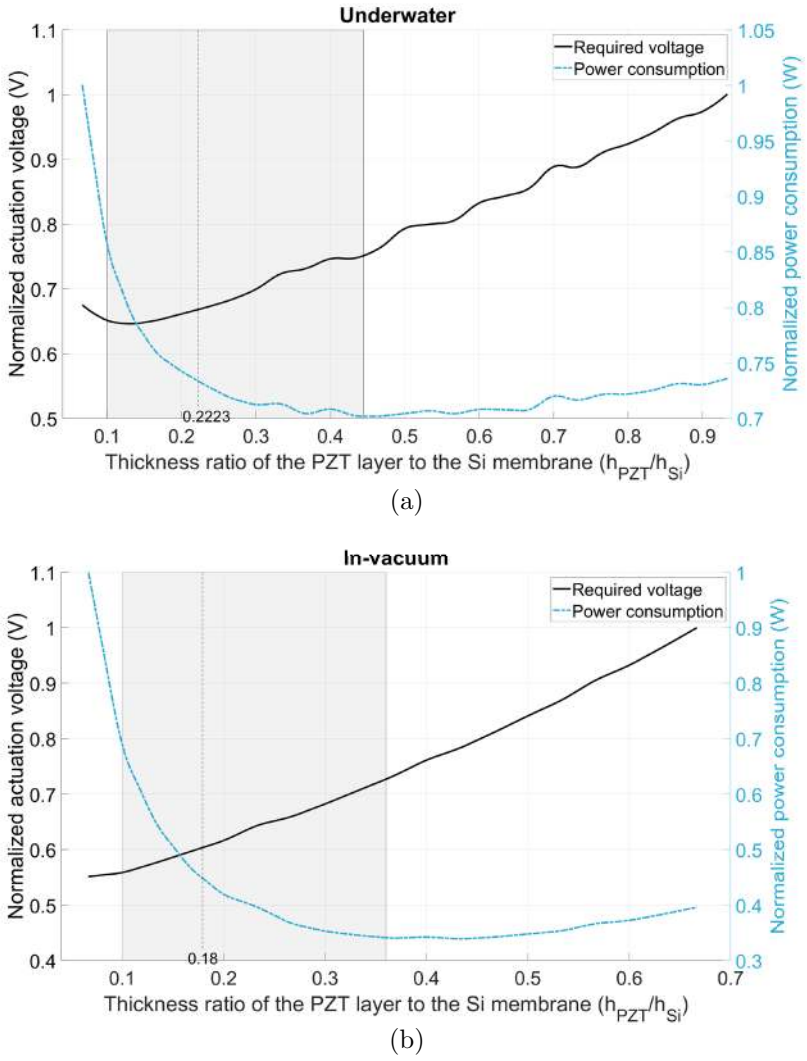

Figure 3. FEM simulation of the required actuation voltage and the power consumption of a pMUT; (a) the underwater simulation aiming a constant pressure of 6 kPa at 1 cm from the surface of the transducer; (b) in vacuum simulation aiming a constant displacement.

for a pMUT with a thickness of 5–10 μm and 1 μm PZT layer, a membrane radius of smaller than 210 μm can keep the frequency variation below 20%.

2.1.2. Optimizing the thickness of the PZT layer. The thickness of the PZT layer has two effects on the response of a pMUT. Firstly, a thicker PZT layer tends to improve the crystal quality and consequently, the piezoelectric coefficient. Secondly, the thickness of the PZT layer has a direct relationship with the generated force or the applied bending moment on the membrane. A thicker PZT layer results in a higher bending moment [31, 32]. These two effects point toward a thicker PZT layer. On the other hand, a thick PZT layer has two disadvantages: first, by making the PZT layer thicker, the position of the neutral axis shifts from the center of the Si membrane toward the center of the PZT layer. This degrades the bending moment significantly. Second a thicker PZT layer requires a higher electric field (applied voltage) to induce the desired bending moment.

Moreover, the thickness of the PZT layer has direct effect on the power consumption of the pMUT. The power consumption is calculated by equation (7), in which V is the actuation voltage, Z the amplitude of the input electrical impedance of the pMUT at the working frequency f, θ the angle between the actuation voltage and current, and C_0 the static (DC) input electrical capacitance. By decreasing the thickness of the PZT layer C_0 increases, which leads to the increase of the power consumption. On the other hand, increasing the thickness of the PZT layer reduces C_0; however, a higher voltage is required to actuate the pMUT, which increases the power consumption as well.

$$P = \frac{1}{2}\frac{V^2}{Z}\cos\theta + \frac{1}{2}V^2 f C_0. \tag{7}$$

Therefore, the thickness of the PZT layer should be optimized to compromise between the minimum actuation voltage and power consumption for a specific displacement or output pressure. Figure 3 shows the FEM simulation of the required voltage and power with respect to the ratio of the thickness of the PZT layer to the Si membrane ($h_r = h_{\mathrm{PZT}}/h_{\mathrm{Si}}$). The simulation was performed one time underwater with the aim to achieve a constant pressure of 6 kPa at 1 cm from the

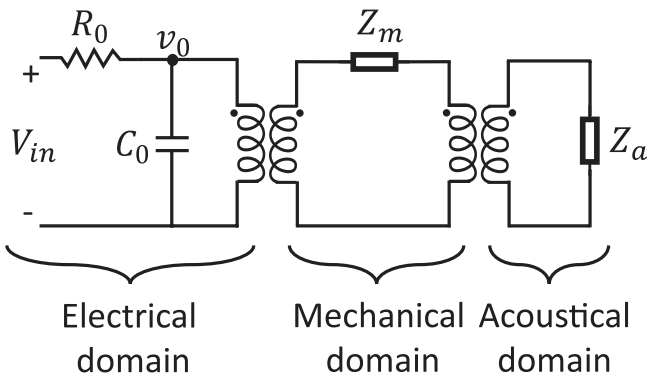

Figure 4. Equivalent electrical model of a pMUT.

surface of the pMUT and the other time in vacuum aiming at a constant displacement. No residual stress was considered. In this optimization process, the resonance frequency might be selected as a flexible parameter, since it varies by alternating the thickness of the PZT layer.

Figure 4 shows the equivalent electrical model of a pMUT, which consists of an electrical domain and mechanical-acoustical domain [33]. R_0 is the parasitic resistor of the top electrode and bond-wires. As shown, increasing C_0 decreases the input impedance, which means that most of the input electrical power is consumed to charge and discharge of C_0. This consumed power is called dynamic power consumption and is shown by the second term of equation (7).

The first term of equation (7) is the power consumed by the resistive part of the pMUT impedance and is dependent to the working medium, since the loading from the medium alters the impedance. Therefore, the results of underwater and in-vacuum simulation are different. Ideally, a pMUT that works in vacuum consumes only the dynamic power and the first term of equation (7) is zero, which means that the impedance is fully imaginary.

The gray part in figure 3 is the area where, depending on the application, the design parameters should be chosen from. The maximum h_r is the point where the power consumption is minimum. Theoretically, the minimum thickness of the PZT layer may converge to zero, but because of practical reasons $h_r = 0.1$ was selected as the minimum value. In practice, a PZT layer with a thickness of less than 500 nm deposited by a sol-gel process, is vulnerable to pin-holes and cracks, which can cause a short-circuit between the top and bottom electrodes. Moreover, the crystal orientation of the PZT layer is enhanced with increased thickness.

Half of the maximum value of h_r, which is the average value between the maximum and minimum power consumption, can be considered as the optimum value of h_r; thus, a thickness ratio of 0.22 and 0.18 were chosen as the optimum values for underwater and in-vacuum pMUTs, respectively. It should be noted that the overall generated bending moment in a pMUT membrane with constant radius of curvature only depends on the thickness of each layer [34]. Accordingly, the optimum PZT thickness is only dependent on the thickness of the Si membrane, in order to generate the maximum bending moment. If the pMUT is intended to be used for energy harvesting applications, the thickness of the PZT should be chosen for minimum power consumption to maximum the generated charge by a constant displacement. Therefore, for underwater and in-vacuum applications the thickness ratio of the PZT to the Si layer should be about 0.45 and 0.38, respectively.

2.1.3. Top electrode dimension optimization. In this section, the optimization of the dimension of the top electrode, as shown in figure 1(a), is discussed. As referred in the introduction, there have been extensive analytical studies on the optimization of the top electrode of a circular piezoelectric pMUT. In most publications, it was assumed that all layers on the membrane are without residual stress. Thus, the optimum size of the top electrode was found to be equal to the area of the membrane where there is no sign change of the stress during the deflection. This area has a radius of $\frac{\sqrt{2}}{2}a$. However, in a real pMUT this is not completely correct, since the deposition of metal and PZT layers always result in some residual stress. In order to study the dynamic behavior of a pMUT through optimizing the dimension of the top electrode for the maximum displacement, the vibration of a pMUT with a pre-stressed PZT layer was modeled by FEM simulation. Accordingly, a pMUT with a radius of 205 μm and 6 μm thick Si was studied by alternating the residual stress of a 1 μm deposited PZT layer. The pMUT was aimed to have a resonance frequency of about 500 kHz, while the PZT layer had no residual stress. The thickness and radius of the Si membrane were chosen based on section 2.1.1 in order to have a low dependency of the resonance frequency to the residual stress and in the same time maximize the output acoustic pressure. As in the previous section, the residual stress of the PZT layer was modeled as thermal stress. Figure 5(a) shows the optimum ratio of the electrode radius to the radius of the membrane at its resonance frequency. As mentioned in section 2.1.1, the resonance frequency of a pMUT depends on the residual stress of the deposited layers. Figure 5(b) shows the resonance frequency with respect to the residual stress of the PZT layer.

The existence of residual stress in the PZT layer generates a bending moment in the pMUT membrane, which results in membrane buckling. The buckling amplitude of the membrane as a function of the residual stress of the PZT layer is shown in figure 5(b). When the residual stress in the PZT layer becomes compressive, the effective flexural rigidity commences to decline [35]. As a result, the resonance frequency drops. The reduction in the effective flexural rigidity continues until the buckling amplitude is more than about 2.1% of the membrane thickness. Therefore, the static behavior of a pMUT can be distinguished to three categories: (i) the residual stress of the piezoelectric layer is compressive and the buckling amplitude is less than 2.1% of the membrane thickness (green region in figures 5 and 6); (ii) the residual stress of the piezoelectric layer is compressive and the buckling amplitude is more than 2.1% of the membrane thickness (the left-red region in figures 5 and 6); (iii) the residual stress of the piezoelectric layer is tensile (the right, red region in figures 5 and 6).

The green region is the most critical region in the design of a pMUT. As shown in figure 6, by using the optimum top electrode radius the displacement response is significantly higher than using the analytically found radius ($\frac{\sqrt{2}}{2}a$). Therefore, if

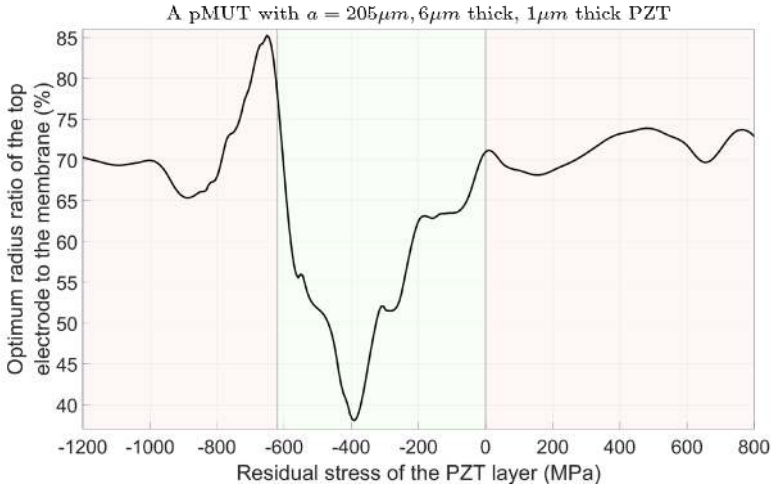

(a)

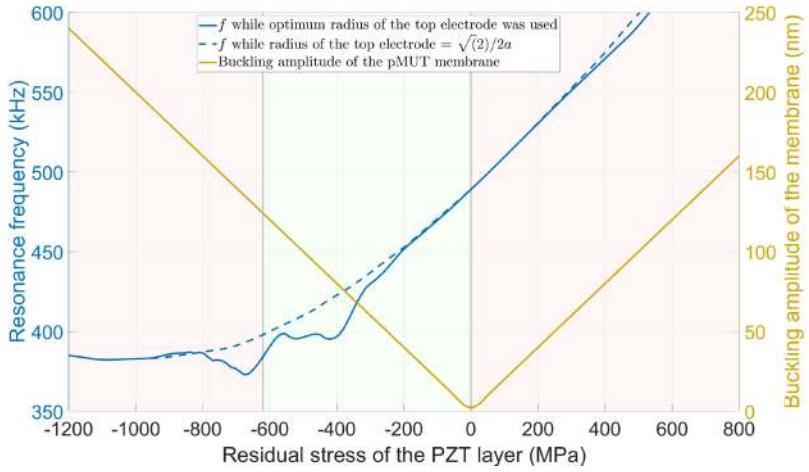

(b)

Figure 5. (a) FEM simulation of the optimum radius of the top electrode to have the maximum displacement as a function of the residual stress of the PZT layer. (b) The resonance frequency variation with respect to the residual stress while the optimum electrode radius and the radius of $\frac{\sqrt{2}}{2}a$ were used. The buckling amplitude of the membrane as a function of the PZT residual stress is also shown on the right y-axis.

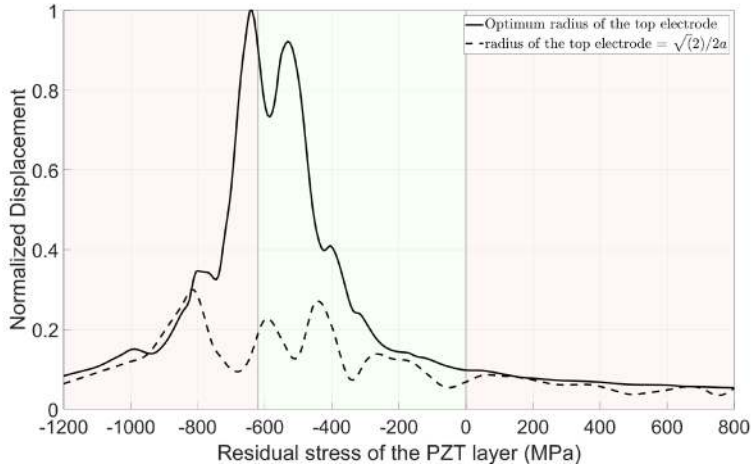

Figure 6. Normalized displacement amplitude of the pMUT as a function of residual stress of the PZT layer, while the optimum electrode radius and the radius of $\frac{\sqrt{2}}{2}a$ was used.

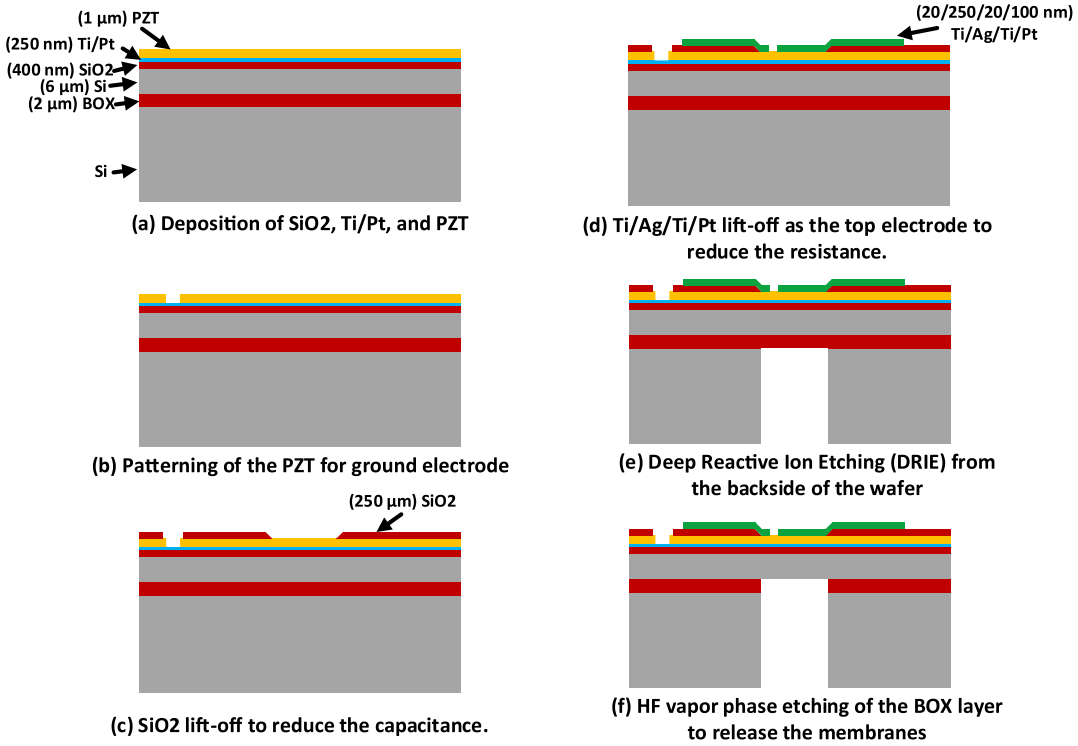

Figure 7. Fabrication process flow of the pMUT; (a) the deposition of the SiO_2, Ti/Pt, and the PZT layer; (b) the wet etching of the PZT layer to access to the bottom electrode; (c) the sputtering and lift-off of a SiO_2 layer as an insulator between the PZT and top electrode to reduce parasitic capacitance; (d) the lift-off of Ti/Ag/Ti/Pt as the top electrode; (e) the pMUT membrane was realized by DRIE from the backside of the wafer. The box layer was used as the etch stop; (f) the box is removed by HF vapor phase etching to release the pMUT membrane.

the fabricated pMUT remains in the green region, an average value of 57%a should be selected as the top electrode radius.

It was also found from figure 5(b) that in the green region the resonance frequency varies by changing the radius of the top electrode. This means that the flexural rigidity in dynamic mode is different from the static mode and is dependent on the geometrical form of the electrical actuation. This phenomenon will be shown in practice in section 2.3.

The other technique in the design of the top electrode, which improves the FOM, is to cover the circumferential part of the membrane, where the stress has an opposite sign with respect to the central part, by a ring electrode, as shown in figure 1(b). Then, the ring electrode can be actuated with a phase shift to generate a reverse lateral stress with respect to the central electrode. This technique was reported in previous works and will be discussed in more detail in section 3 [9, 22, 23].

2.2. pMUT fabrication

As mentioned earlier, a pMUT with a resonance frequency of approximately 500 kHz is selected to be fabricated, which is intended to be used in underwater and in-air sensor networks applications. Moreover, a pMUT with 500 kHz resonance frequency allows us to study the effect of the residual stress in more details. Therefore, according to the design parameters discussed in section 2.1, a pMUT with a Si membrane thickness of 6 μm, a radius of 205 μm, and a 1 μm thick PZT layer was fabricated. The fabrication process is shown in figure 7. First, about 400 nm thermal SiO_2 was grown on the device layer of a silicon-on-insulator (SOI) wafer. Then, 20 nm Ti and 250 nm Pt were deposited by RF sputtering. The Pt was deposited at 200 W RF power, 10.2 μbar process pressure, and with 25 sccm Ar flow, in order to have almost zero residual stress. A comprehensive study on the residual stress of sputtered Pt was performed by Hoffman *et al* [36]. A 1 μm PZT layer was deposited on top of the SiO_2/Ti/Pt layer by sol-gel process [23]. Then, the PZT was patterned to access the bottom electrode. Thereafter, the top electrode metal layer was sputtered and patterned. Finally, the membrane was released by deep reactive ion etching (DRIE) from the backside of the wafer until the buried oxide layer (BOX), and consecutively removing the BOX by HF vapor etching, while the front side of the wafer was protected.

The applied bending moment on the membrane is directly proportional to the electric field around the PZT layer, which is defined by the voltage across C_0 in the equivalent electrical model of the pMUT, figure 4. However, R_0 and C_0 form a low-pass filter with a bandwidth of $1/(R_0C_0)$ at the node v_0 in the model. It is extremely important that the 3 dB bandwidth of the unwanted lowpass filter be higher than the mechanical resonance frequency of the pMUT; otherwise, the received voltage, and accordingly the electric field around C_0, is degraded and the bending moment is reduced. In other words, the displacement or the velocity per volt of the pMUT is decreased. Basically, the R_0C_0 time constant does not allow

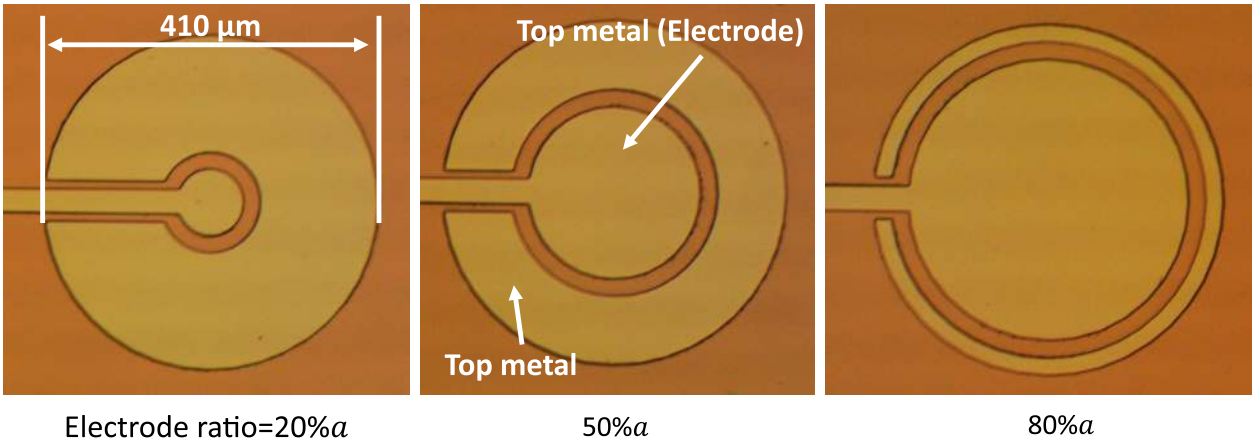

Figure 8. Optical microscopy of three pMUTs with 20%, 50%, and 80% ratio of the top electrode to the pMUT membrane radius.

C_0 be fully charged and the PZT layer reach to its maximum strain. Thus, only a small fraction of input electrical power is transferred to the mechanical-acoustical domain.

The parasitic resistor (R_0) is mainly due to the resistance of the top electrode and the metal track from the electrode to the bond-pad. The parasitic capacitor (C_0) results from the capacitance between the top and the bottom electrode, with the PZT layer acting as an insulator. Due to the high permittivity of the PZT, C_0 has an impressive capacitance value. Consequently, to reduce R_0 a stack of Ti/Ag/Ti/Pt with thicknesses of 20 nm/250 nm/20 nm/100 nm, respectively, were deposited and patterned by a lift-off process as the top electrode. Moreover, step (c) is added in the fabrication process in figure 7, in order to reduce C_0 of the pMUT. As shown, a 250 nm SiO_2 was sputtered between the PZT and the top electrode, except on top of the pMUT membrane. Since the permittivity of SiO_2 is much lower than of PZT, the electric field concentrates in the SiO_2 layer and C_0 decreases. A low R_0C_0 time constant is indispensable in the design and fabrication of large pMUTs or pMUT in array configuration when many of them are actuated simultaneously. In addition, a low C_0 improves the signal to noise ratio of the pMUT as an ultrasound receiver.

2.3. Results and discussion of the fabricated pMUT with architecture (a)

The proposed pMUT with optimized design parameter was fabricated by varying the radius of the top electrode from 20% up to 100% of the radius of the pMUT membrane. Different dimensions of the top electrode cause different residual stress distributions on the membrane, which affect the resonance frequency. In order to make the resonance frequency of the membrane independent from the top electrode dimension, the entire membrane was covered by the metal layer of the top electrode. Figure 8 shows an optical microscopy image of three pMUTs with 20%, 50%, and 80% ratio of the top electrode to the pMUT membrane radius. A gap of 20 μm between the electrode and the covering metal layer was taken into account. All pMUTs were polled at room temperature, by 25 V for 15 s. The total residual stress of the deposited PZT layer in combination with both bottom and top electrodes was measured by the curvature of the wafer—prior to any patterning—and using Stoneys equation to be equal to −650 MPa. The buckling of the membrane was measured by a stylus profilometer (Bruker DektakXT, Billerica, Massachusetts, United States) to be 160 nm. By comparing the measured residual stress and the buckling of the membrane to the simulation results of figure 5, it is expected to have an optimum radius that is larger than the radius obtained by analytical analysis ($\frac{\sqrt{2}}{2}a$).

More than ten batches of pMUTs distributed uniformly on the wafer were measured to reduce the impact of process variations on the results. The displacement response (before and after polling of the PZT layer) and the resonance frequency of each pMUT were measured by a laser doppler vibrometer (LDV) (Polytec MSA-500, Waldbronn, Germany) and are shown in figure 9. The polled pMUT shows the maximum displacement response of 6.6 μm V^{-1} at a top electrode radius of 80%a. The non-polled pMUT had a considerable displacement response of 4.5 μm V^{-1}. The resonance frequency remained constant before and after polling of the PZT layer. Moreover, the resonance frequency, regardless of the residual stress of the top electrode, reduced while the top electrode radius became larger than 60%a. This phenomenon was confirmed by comparing the resonance frequency of the optimum electrode radius and the radius of $\frac{\sqrt{2}}{2}a$ by FEM simulations shown in figure 5(b).

3. Architecture (b): using center and ring top electrodes

As mentioned in section 2.1.3, one of the techniques to improve the displacement response of a pMUT is to cover the circumferential part of the membrane, where the stress has an opposite sign with respect to the central part, by a ring electrode, as shown in figure 1(b). The induced stress by the ring electrode on the membrane compared to the center electrode should have a 180° phase shift. Therefore, the phase of the applied signal to the ring electrode should be shifted with respect to the center electrode, but not necessarily 180°, as the

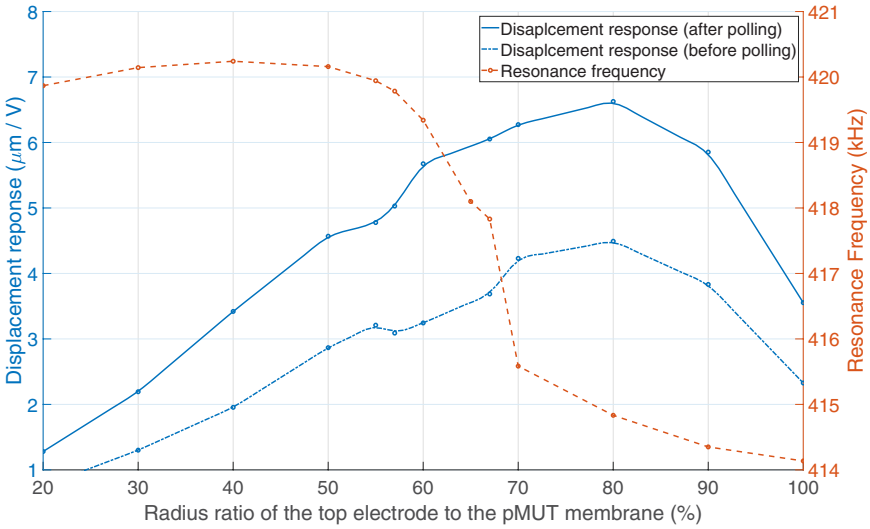

Figure 9. Measured displacement response and the resonance frequency of several pMUTs as a function of the radius ratio of their top electrode to the pMUT membrane.

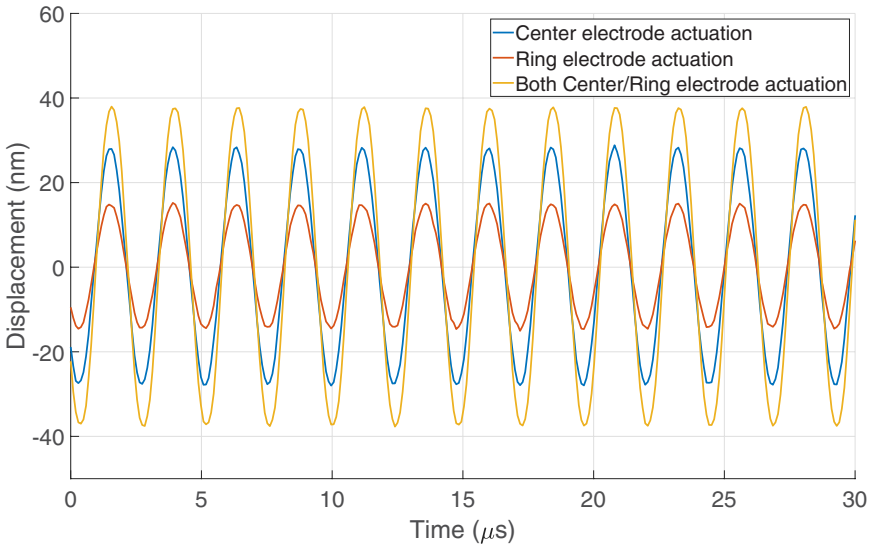

Figure 10. In-air displacement of a pMUT to a 10 mV_{p-p} sinus signal by using only the center electrode, ring electrode, and both center/ring electrode. The center electrode had a radius of 55%a and the width of the ring electrode was 45 μm.

electrical impedance of the ring electrode can be different from the center electrode. This means that the applied voltage over the pMUT through the center electrode may have different phase angle with respect to the ring electrode. The electrical impedance depends on the input electrical DC capacitance and resistance, mechanical parameters, and loading of the working medium, as shown in figure 4. For a big pMUT or a pMUT array operating in air or vacuum, the input capacitance is more pronounced than the mechanical parameters or the loading effect of the medium. Therefore, the phase shift over the pMUT capacitor (C_0) can be calculated by:

$$\varphi = -\arctan(2\pi f R_0 C_0) \tag{8}$$

where f is the mechanical resonance frequency. As a result, the required phase shift of the applied signal to the ring electrode with respect to the center electrode can be calculated as:

$$\phi = \pm 180^\circ + (\varphi_c - \varphi_r) \tag{9}$$

where φ_c and φ_r are the phase angles of the applied current to the center and ring electrode, respectively.

Figure 10 shows the in-air displacement of a pMUT to a 10 mV_{pp} sinusoidal signal by using the center electrode, ring electrode, and both the center/ring electrodes. The center electrode of the measured pMUT had a radius of 68%a and $C_{0,center} = 1.07$ nF. The ring electrode had a width of 45 μm and $C_{0,ring} = 0.96$ nF. The measured R_0 of the pMUT from the bond-pad to the membrane was about 4 Ω. Since the fabricated device was measured in air, the effect of the medium was not significant on the device. Therefore, the required phase shift of the applied signal to the ring electrode with respect to the center electrode can be calculated by equation (9). However, because of the negligible difference between the value of $C_{0,center}$ and $C_{0,ring}$ as well as the small value of R_0, the required phase shift is about 180°. The phase shift was adjusted by a waveform generator (Agilent 33500B series, Agilent technologies, Santa Clara, California, USA).

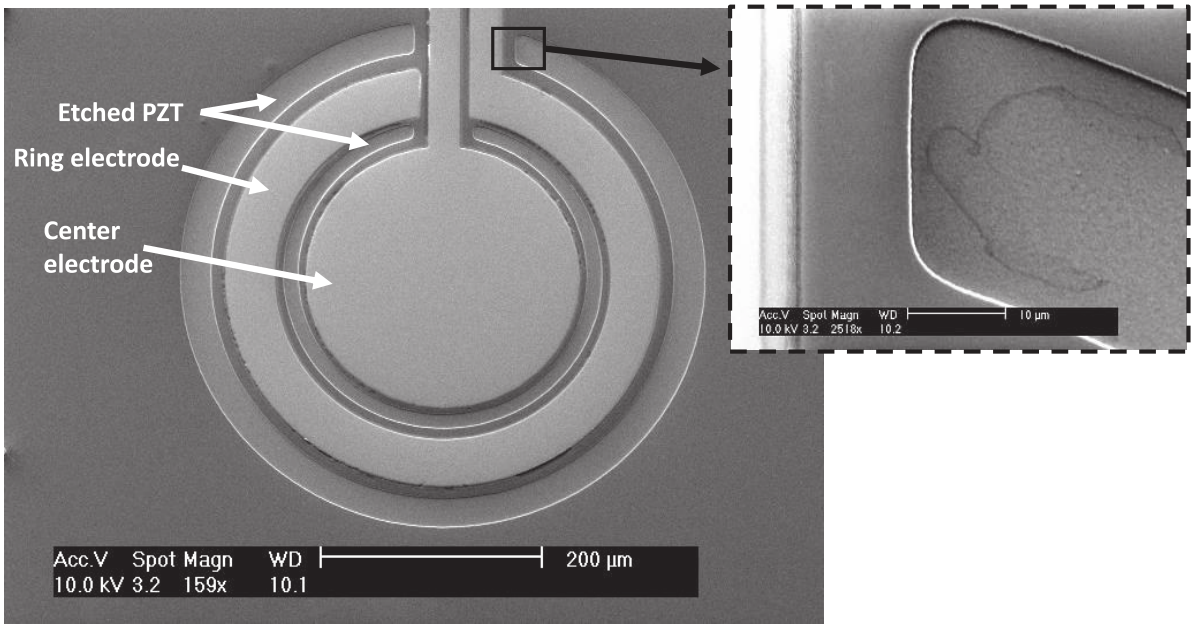

Figure 11. SEM image of a fabricated pMUT with etched PZT, which its graphical illustrated is showin in figure 1(c).

Sample	(i)	(ii)	(iii)	(Reference)
	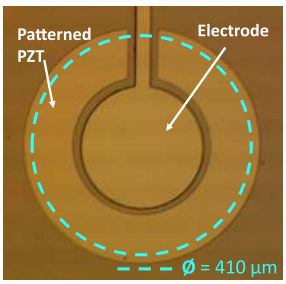	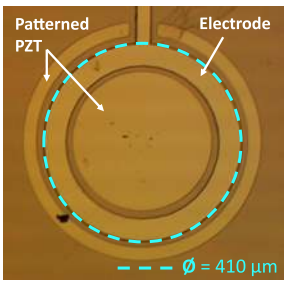	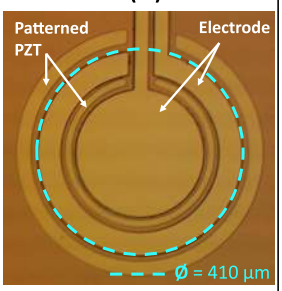	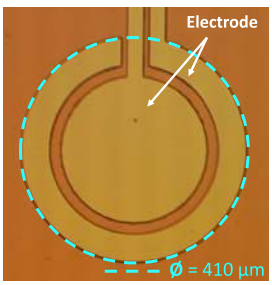
Resonance frequency	395 kHz	484 kHz	423 kHz	418 kHz
Displacement response	7.4 µm/V	3.66 µm/V	8.6 µm/V	5.6 µm/V (Center) 3.0 µm/V (Ring) 7.5 µm/V (Both)
Q-factor	143	90	110	104

Figure 12. Optical microscopy of different pMUTs with patterned PZT layer and their measured resonance frequency, displacement response, and Q-factor. The PZT layer in the reference sample was not patterned. The perimeter of each pMUT membrane is shown by dashed line.

As shown in figure 10, by using both electrodes the displacement response was improved by 35%, which corresponds to 7.5 μm V^{-1}.

4. Architecture (c): a pMUT with a patterned PZT layer

Besides the discussed techniques during the design and fabrication of a pMUT to improve its performance, this section introduces another technique in the fabrication, which improves the displacement response significantly.

The fabricated pMUTs in sections 2 and 3 consist of a PZT layer that uniformly covered the whole wafer. However, by patterning the PZT layer on the circumferential area of the top electrode (center or ring electrode), the fixed boundary condition on the PZT layer is removed and a stronger electromechanical coupling is induced. Therefore, the displacement response can be improved, since a larger bending moment is generated by actuating the pMUT. However, by patterning the PZT, its residual stress is released and transferred to a bending moment, which results in a different stress distribution through the thickness of the membrane. This would create a larger buckling, change the effective flexural rigidity, and affect the resonance frequency.

Figure 1(c) shows the most complex form of this technique, where the PZT layer is patterned in between the ring and center electrodes, as well as on the perimeter of the pMUT membrane. The fabrication process of a pMUT with patterned PZT layer is the same as the process explained in section 2.2. Figure 11 shows the SEM image of a fabricated pMUT with etched PZT, as illustrated in figure 1(c).

In order to investigate the effect of patterning the PZT layer on the performance of the pMUT in more details, architecture (c) in figures 1(c) and 11 was split into two different layouts.

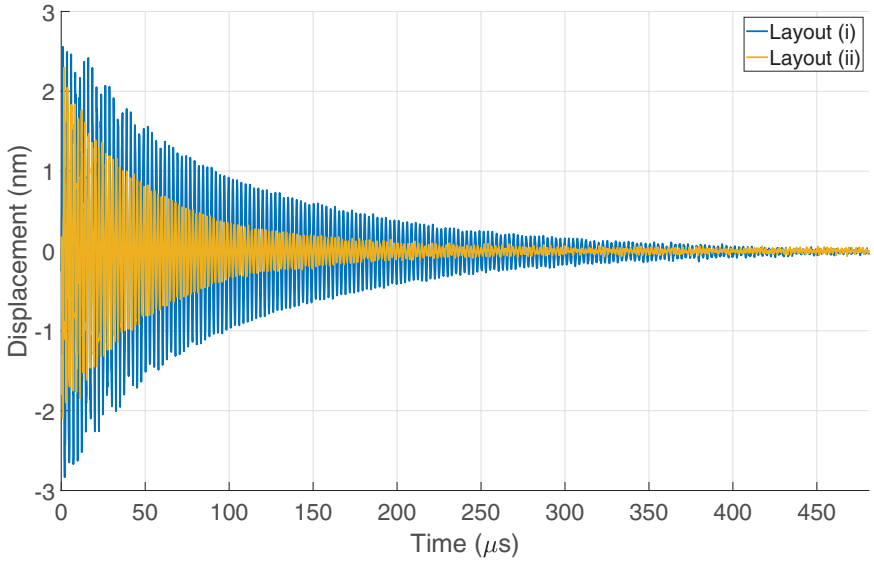

Figure 13. Impulse response of the pMUTs with layouts (i) and (ii). The applied impulse had a width of 100 ns and an amplitude of 200 mV.

Table 2. Comparison between the performance of the proposed pMUT in this paper, which was designed and fabricated by the discussed strategy, and the state-of-the-art.

	PMUT's shape	Piezoelectric material	f_r (kHz)	Displacement response (nm V^{-1})	Velocity (mm/s/V)	Comments
This work	**Circular**	**PZT**	**423**	**8600**	**22 860**	
[24]	Circular	Fibered epitaxial PZT	7300	1.3	29.8	
[37]	Rect.	PZT	230	5000	7220	Using DC bias
[37]	Rect.	PZT	185	2000	2324	No DC bias
[38]	Circular	PZT	46	169	48.8	Using DC & pressure bias
[39]	Square	PZT	766	50.8	244.5	
[18]	Circular	PZT	11 000	316	21 800	
[40]	Square	PZT	119	1420	1062	
[41]	Rect.	PZT	5500	500	17 280	Using DC bias
[22]	Circular	PZT	12 000	160	12 063	
[17]	Circular	GSV PZT	300.9	455	430	
[42]	Square	PZT	57.75	297	53.9	

The first layout has a center electrode with a radius of 68%a and the second layout has a ring electrode with a width of 45 μm. In both layouts the PZT layer was etched except where the top electrode located. The combination of the first and second layout results in the third layout, which is shown in figure 11. All layouts are shown in figure 12.

In the layouts (i), where a center electrode was used, the displacement response and Q-factor was increased by 32% with respect to the reference pMUT with non-patterned PZT when actuated by the center electrode. The absence of the center top electrode as well as the central PZT layer in layout (ii), removes the excessive residual stress on the membrane. In this case the effective flexural rigidity and, therefore, the resonance frequency was higher compared to the layouts (i). The higher flexural rigidity increased the damping ratio and reduced the Q-factor as well. The displacement response of layout (ii) improved by 22% with respect to the reference layout when actuated by the ring electrode. The third layout, which obtained by combining layouts (i) and (ii), resulted in the highest displacement response of 8.6 μm V^{-1} and a Q-factor of 110 in air. The displacement response of the third layout improved by 17% with respect to the reference layout when actuated by both center and ring electrode.

It should be noted that, if the piezoelectric layer was already under strong compressive stress, resulting in buckling of the membrane more than 2.1% of its thickness, etching the piezoelectric layer has the tendency to increase the effective flexural rigidity and not necessarily improves the pMUT displacement response. In a worst-case scenario, the induced buckling by etching the piezoelectric layer may break the membrane.

The Q-factor in the aforementioned samples was approximated by the number of rings (N) in their impulse response, at which the ringing amplitude falls below 5% of the maximum value. The impulse response of each pMUT was measured by applying a rectangular pulse with a width of 100 ns and amplitude of 200 mV. As a matter of comparison, the impulse response of the samples with layouts (i) and (ii) are shown in figure 13.

5. Conclusion

All major aspects in the design, fabrication, and characterization of a PZT-based pMUT were presented in this paper. The optimum thickness of the PZT layer, top electrode radius, and the effect of residual stress on the resonance of a pMUT were investigated by FEM simulation. It was shown that a thicker PZT layer reduces the power consumption, although it increased the required actuation voltage amplitude. For in-vacuum and underwater pMUTs, a PZT thickness of $0.18h_{Si}$ and $0.22h_{Si}$ can be used, respectively, in order to compromise between the power consumption and actuation voltage amplitude. It was shown that the optimum top electrode radius depends on the residual stress of the PZT and metal layers. As such, if the deposited layers have compressive stress and the membrane buckling is less than 2.1%t, a top electrode with a radius of 57%a should be used. Otherwise, a top electrode with a radius of 70%a is suitable.

Based on the design strategy, a 500 kHz pMUT was fabricated in three different architecture: (i) a pMUT with a top center electrode, (ii) a pMUT with a top center and ring electrode, (iii) a pMUT with a patterned PZT layer. All three pMUT architectures were fabricated and their displacement response, resonance frequency, and Q-factor were compared. The fabricated pMUT in all three architectures had a radius of 205 μm, a Si membrane thickness of 6 μm, and PZT thickness of 1 μm. The second and third architectures improved the displacement response of a pMUT compared to the first architecture by 35% and 32%, respectively.

The maximum displacement response of 8.6 μm V^{-1} obtained from the third architecture with two center/ring top electrodes and a patterned PZT layer, which was 91% higher than the non-polled pMUT with architecture (a).

Acknowledgments

This work was funded by the FP7 European Research Council (FP7/2007-2013)/ERC Grant agreement No. 340931, and the Horizon 2020 FET-Open innovation program under Grant agreement No. 665347, Phoenix.

ORCID iDs

S Sadeghpour https://orcid.org/0000-0002-7575-2763

References

[1] Wildes D *et al* 2016 4D ice: a 2D array transducer with integrated asic in a 10-fr catheter for real-time 3D intracardiac echocardiography *IEEE Trans. Ultrason. Ferroelectr. Freq. Control* **63** 2159–73

[2] Sadeghpour S, Meyers S, Kruth J-P, Vleugels J, Kraft M and Puers R 2019 Resonating shell: a spherical-omnidirectional ultrasound transducer for underwater sensor networks *Sensors* **19** 757

[3] Wang T, Kobayashi T, Yang B, Wang H and Lee C 2016 Highly sensitive piezoelectric micromachined ultrasonic transducer (pMUT) operated in air 2016 *IEEE 11th Annual International Conference on Nano/Micro Engineered and Molecular Systems (NEMS)* pp 294–9

[4] Lu Y, Heidari A and Horsley D A 2014 A high fill-factor annular array of high frequency piezoelectric micromachined ultrasonic transducers *J. Microelectromech. Syst.* **24** 904–13

[5] Zhou Q, Lam K H, Zheng H, Qiu W and Shung K K 2014 Piezoelectric single crystal ultrasonic transducers for biomedical applications *Prog. Mater. Sci.* **66** 87–111

[6] Jiang X, Tang H-Y, Lu Y, Ng E J, Tsai J M, Boser B E and Horsley D A 2017 Ultrasonic fingerprint sensor with transmit beamforming based on a PMUT array bonded to CMOS circuitry *IEEE Trans. Ultrason. Ferroelectr. Freq. Control* **64** 1401–8

[7] Zhou Z, Yoshida S and Tanaka S 2017 Epitaxial PMNN-PZT/SI MEMS ultrasonic rangefinder with 2 m range at 1 V drive *Sensors Actuators* A **266** 352–60

[8] Yeh D T, Oralkan O, Wygant I O, O'Donnell M and Khuri-Yakub B T 2006 3D ultrasound imaging using a forward-looking cmut ring array for intravascular/intracardiac applications *IEEE Trans. Ultrason. Ferroelectr. Freq. Control* **53** 1202–11

[9] Sadeghpour S, Lips B, Kraft M and Puers R 2019 Flexible soi-based piezoelectric micromachined ultrasound transducer (PMUT) arrays *20th Int. Conf. on Solid-State Sensors, Actuators and Microsystems (TRANSDUCERS)* 250–3

[10] Dausch D E, Gilchrist K H, Carlson J B, Hall S D, Castellucci J B and von Ramm O T 2014 *In vivo* real-time 3D intracardiac echo using pmut arrays *IEEE Trans. Ultrason. Ferroelectr. Freq. Control* **61** 1754–64

[11] Sadeghpour S, Kraft M and Puers R 2018 pMUTS array with dynamic directivity: a study of its underwater acoustic power intensity *IEEE Int. Ultrasonics Symp.* (IEEE) pp 1–9

[12] Kusano Y, Wang Q, Luo G-L, Lu Y, Rudy R Q, Polcawich R G and Horsley D A 2018 Effects of dc bias tuning on air-coupled pzt piezoelectric micromachined ultrasonic transducers *J. Microelectromech. Syst.* **27** 296–304

[13] Chen X, Liu X, Wang T, Le X, Ma F, Lee C and Xie J 2018 Piezoelectric micromachined ultrasonic transducers with low thermoelastic dissipation and high quality factor *J. Micromech. Microeng.* **28** 057001

[14] Akasheh F, Fraser J D, Bose S and Bandyopadhyay A 2005 Piezoelectric micromachined ultrasonic transducers: modeling the influence of structural parameters on device performance *IEEE Trans. Ultrason. Ferroelectr. Freq. Control* **52** 455–68

[15] Wang T, Sawada R and Lee C 2015 A piezoelectric micromachined ultrasonic transducer using piston-like membrane motion *IEEE Electron Device Lett.* **36** 957–9

[16] Wang M and Zhou Y 2017 Design of piezoelectric micromachined ultrasonic transducers (PMUTS) for high pressure output *Microsyst. Technol.* **23** 1761–6

[17] Jung J, Annapureddy V, Hwang G-T, Song Y, Lee W, Kang W, Ryu J and Choi H 2017 31-mode piezoelectric micromachined ultrasonic transducer with PZT thick film by Granule spraying in vacuum process *Appl. Phys. Lett.* **110** 212903

[18] Lu Y and Horsley D A 2015 Modeling, fabrication, and characterization of piezoelectric micromachined ultrasonic transducer arrays based on cavity soi wafers *J. Microelectromech. Syst.* **24** 1142–9

[19] Sammoura F, Smyth K and Kim S-G 2013 Optimizing the electrode size of circular bimorph plates with different boundary conditions for maximum deflection of piezoelectric micromachined ultrasonic transducers *Ultrasonics* **53** 328–34

[20] Mo C, Wright R, Slaughter W S and Clark W W 2006 Behaviour of a unimorph circular piezoelectric actuator *Smart Mater. Struct.* **15** 1094
[21] Jung J, Lee W, Kang W, Shin E, Ryu J and Choi H 2017 Review of piezoelectric micromachined ultrasonic transducers and their applications *J. Micromech. Microeng.* **27** 113001
[22] Lu Y, Wang Q and Horsley D A 2015 Piezoelectric micromachined ultrasonic transducers with increased coupling coefficient via series transduction *IEEE Int. Ultrasonics Symp.* (IEEE) pp 1–4
[23] Sadeghpour S and Puers R 2018 Optimization in the design and fabrication of a PZT piezoelectric micromachined ultrasound transducer (PMUT) *Multidisciplinary Digital Publishing Institute Proc.* **2** 743
[24] Ngoc Thao P, Yoshida S and Tanaka S 2018 Fabrication and characterization of PZT fibered-epitaxial thin film on SI for piezoelectric micromachined ultrasound transducer *Micromachines* **9** 455
[25] Blevins R D 1979 Formulas for natural frequency and mode shape (Malabar, FL: Kreiger Publishing)
[26] Sandberg R, Svendsen W, Mølhave K and Boisen A 2005 Temperature and pressure dependence of resonance in multi-layer microcantilevers *J. Micromech. Microeng.* **15** 1454
[27] Kinsler L E, Frey A R, Coppens A B and Sanders J V 1999 Fundamentals of acoustics *Fundamentals of Acoustics* 4th edn, ed E Lawrence *et al* (New York: Wiley) p 560
[28] Sadeghpour S, Kraft M and Puers R 2019 Highly efficient piezoelectric micromachined ultrasound transducer (PMUT) for underwater sensor netwroks *20th Int. Conf. on Solid-State Sensors, Actuators and Microsystems (TRANSDUCERS)* 162–5
[29] Wang M, Zhou Y and Randles A 2016 Enhancement of the transmission of piezoelectric micromachined ultrasonic transducer with an isolation trench *J. Microelectromech. Syst.* **25** 691–700
[30] Peake W H and Thurston E G 1954 The lowest resonant frequency of a water-loaded circular plate *J. Acoust. Soc. Am.* **26** 166–8
[31] Kim S, Clark W W and Wang Q-M 2005 Piezoelectric energy harvesting with a clamped circular plate: analysis *J. Intell. Mater. Syst. Struct.* **16** 847–54
[32] Sader J E 2001 Surface stress induced deflections of cantilever plates with applications to the atomic force microscope: rectangular plates *J. Appl. Phys.* **89** 2911–21
[33] Przybyla R J, Shelton S E, Guedes A, Izyumin I I, Kline M H, Horsley D A and Boser B E 2011 In-air rangefinding with an ALN piezoelectric micromachined ultrasound transducer *IEEE Sensors J.* **11** 2690–7
[34] Malinauskas K, Ostaševičius V, Daukševičius R and Grigaliūnas V 2012 Residual stress in a thin-film microoptoelectromechanical (MOEMS) membrane *Mechanics* **18** 273–9
[35] Brand O, Hornung M, Baltes H and Hafner C 1997 Ultrasound barrier microsystem for object detection based on micromachined transducer elements *J. Microelectromech. Syst.* **6** 151–60
[36] Hoffman D and Thornton J A 1982 Internal stresses in CR, MO, TA, and PT films deposited by sputtering from a planar magnetron source *J. Vac. Sci. Technol.* **20** 355–8
[37] Kusano Y, Wang Q, Rudy R Q, Polcawich R G and Horsley D A 2017 Wideband air-coupled pzt piezoelectric micromachined ultrasonic transducer through DC bias tuning *IEEE 30th Int. Conf. on Micro Electro Mechanical Systems* (IEEE) pp 1204–7
[38] Wang Z, Yao Y, Wang X, Yue W, Chen L and Zhang X X 2013 Bending-induced electromechanical coupling and large piezoelectric response in a micromachined diaphragm *Sci. Rep.* **3** 3127
[39] Ling J, Chen Y-Q, Chen Y, Wang D-Y, Zhao Y-F, Pang Y, Yang Y and Ren T-L 2018 Design and characterization of high-density ultrasonic transducer array *IEEE Sensors J.* **18** 2285–90
[40] Nakamoto S, Sano R, Kanda K, Fujita T and Maenaka K 2018 Multilayer Pb (Zr, Ti) O_3 thin films for ultrasonic transducer *Electron. Commun. Japan* **101** 63–8
[41] Lu Y, Rozen O, Tang H-Y, Smith G L, Fung S, Boser B E, Polcawich R G and Horsley D A 2015 Broadband piezoelectric micromachined ultrasonic transducers based on dual resonance modes *28th IEEE Int. Conf. on Micro Electro Mechanical Systems* (IEEE) pp 146–9
[42] Zhu H, Miao J, Wang Z, Zhao C and Zhu W 2005 Fabrication of ultrasonic arrays with 7 μm PZT thick films as ultrasonic emitter for object detection in air *Sensors Actuators* A **123** 614–9